

# Universal Peptide Hydrogel for Scalable Physiological Formation and Bioprinting of 3D Spheroids from Human Induced Pluripotent Stem Cells

*Quan Li, Guangyan Qi, Xuming Liu, Jianfa Bai, Jikai Zhao, Guosheng Tang, Yu Shrike Zhang, Ruby Chen-Tsai, Meng Zhang, Donghai Wang, Yuanyuan Zhang, Anthony Atala, Jia-Qiang He, and Xiuzhi Susan Sun\**

Human induced pluripotent stem cells (hiPSCs) are used for drug discoveries, disease modeling and show great potential for human organ regeneration. 3D culture methods have been demonstrated to be an advanced approach compared to the traditional monolayer (2D) method. Here, a self-healing universal peptide hydrogel is reported for manufacturing physiologically formed hiPSC spheroids. With 100 000 hiPSCs encapsulated in 500 µL hydrogel, ≈50 000 spheroids mL<sup>-1</sup> (diameter 20–50 µm) are generated in 5 d. The spheroids in the universal peptide hydrogel are viable (85–96%) and show superior pluripotency and differentiation potential based on multiple bio-markers. Cell performance is influenced by the degradability of the hydrogel but not by gel strength. Without postprinting crosslinking aided by UV or visible lights or chemicals, various patterns are easily extruded from a simple star to a kidney-like organ shape using the universal peptide hydrogel bioink showing acceptable printability. A 20.0 × 20.0 × 0.75 mm<sup>3</sup> sheet is finally printed with the universal peptide hydrogel bioink encapsulating hiPSCs and cultured for multiple days, and the hiPSC spheroids are physiologically formed and well maintained.

## 1. Introduction

Stem cells such as human induced pluripotent stem cells (hiPSCs) can self-renew indefinitely in theory and differentiate into almost all somatic cell types; thus, they have attracted increased attention in the research community and have the potential to improve human health.<sup>[1]</sup> In particular, hiPSCs can be derived from patient-specific blood using removable Sendai virus, which provides reliable approaches for disease modeling, drug screening/toxicity testing, personalized cell therapies, and regenerative medicine.<sup>[2]</sup> Over more than a decade, hiPSCs have been cultured as monolayers on flat surfaces (2D) with specifically designed coating materials from mitotically inactivated mouse embryonic fibroblasts<sup>[3]</sup> to Matrigel and extracellular matrix (ECM)

Q. Li, J. Zhao, D. Wang, X. S. Sun  
Department of Biological and Agricultural Engineering  
Kansas State University  
Manhattan, KS 66506, USA  
E-mail: xss@ksu.edu

G. Qi, X. S. Sun  
Department of Grain Science and Industries  
Kansas State University  
Manhattan, KS 66506, USA

X. Liu, J. Bai  
College of Veterinary Medicine  
Kansas State University  
Manhattan, KS 66506, USA

G. Tang, Y. S. Zhang  
Division of Engineering in Medicine  
Department of Medicine  
Brigham and Women's Hospital  
Harvard Medical School  
Cambridge, MA 02139, USA

Y. S. Zhang  
Harvard Stem Cell Institute (HSCI)  
Harvard University  
Cambridge, MA 02138, USA

R. Chen-Tsai  
Applied StemCell, Inc.  
Milpitas, CA 95035, USA

M. Zhang  
Department of Industrial Engineering  
Kansas State University  
Manhattan, KS 66506, USA

Y. Zhang, A. Atala, X. S. Sun  
Wake Forest Institute Regenerative Medicine  
Wake Forest University  
Winston-Salem, NC 27151, USA

J.-Q. He  
Department of Biomedical Sciences and Pathobiology  
Virginia Tech  
Blacksburg, VA 24061, USA

 The ORCID identification number(s) for the author(s) of this article can be found under <https://doi.org/10.1002/adfm.202104046>.

DOI: [10.1002/adfm.202104046](https://doi.org/10.1002/adfm.202104046)

proteins<sup>[4–9]</sup> and then to synthetic polymers and synthetic peptides.<sup>[10–13]</sup> Cells in 2D culture lack an appropriate stem cell niche, which often leads to poor maintenance of pluripotency and inefficient targeted differentiation.<sup>[14]</sup>

Recently, 3D spheroids of pluripotent stem cells (PSCs), including hiPSCs, have been demonstrated to have great potential for hair-bearing human skins.<sup>[15]</sup> Similarly, functional hepatocyte-like organoids were developed using embryoid body spheroids derived from hiPSCs.<sup>[16]</sup> These advances suggested that functional organoids or even whole organs like skin can be possibly generated from hiPSCs. However, these developments are based on spheroids (multicellular aggregates) produced using either nonadherent U-bottom 96-well plates<sup>[15]</sup> or agarose microarray molding plates,<sup>[16]</sup> and differentiation was performed by suspending hiPSC spheroids in medium culture with gentle orbital agitation. These methods are not typically suited for neither tissue engineering through 3D bioprinting technologies nor large-scale manufacturing of physiologically formed hiPSC spheroids for postprinting differentiation as well as many other applications such as drug discoveries and in vitro disease modeling. The microcarrier bead approach has been considered the “3D” method for large-scale cell manufacturing using stirring tank bioreactors,<sup>[17,18]</sup> although it is still based on 2D cell culture principles. Likewise, suspension bioreactors are not ideal for adherent cells such as hiPSCs.<sup>[19]</sup> Neither the microcarrier nor the suspension approach can meet the quality specifications for human PSC 3D spheroid manufacturing described by Lee et al. for the generation of hair-bearing skin<sup>[15]</sup> or Pettinato et al. for differentiation into fully functional liver organoids.<sup>[16]</sup> 3D bioprinting shows potential for high-content production of hiPSC spheroids. Although this technology has been studied in recent years, photopolymerization<sup>[20–25]</sup> or temperature control<sup>[23,26–28]</sup> is often required for postprinting gelation. These conditions oftentimes can be harsh and can harm fragile human PSCs,<sup>[29]</sup> resulting in low viability and insufficient maintenance of pluripotency, and thus, high cell loading densities ranging from  $1 \times 10^7$  to  $1 \times 10^8$  cells mL<sup>-1</sup> are often needed.

Here, we report the development of a scalable and printable universal peptide hydrogel (PGmatrix-M) for highly efficient physiological formation of hiPSC spheroids with superior pluripotency integrity. In parallel, we examined hiPSC spheroids generated in polyethylene glycol (PEG)-based hydrogels and in suspension by nonadherent U-bottom plates. The universal peptide hydrogel was derived from a triblock amphiphilic peptide (h9e)<sup>[30]</sup> with modification. H9e was rationally designed from a group of selective amino acids inspired by two functional native proteins of human muscle and the  $\beta$ -spiral motif of the spider flagelliform silk proteins.<sup>[30,31]</sup> The peptide can self-assemble into nanofibers and then transform into a sol-gel reversible hydrogel by mechanical shearing force under neutral pH at room or physiological temperature.<sup>[32,33]</sup> The h9e hydrogel (PGmatrix) stimulates the secretion of in vivo-like extracellular vesicles<sup>[34]</sup> and thus, we believe that the h9e should be an excellent candidate for high-quality hiPSC spheroid growth. In this study, we initially screened for the “best” culture conditions for physiological formation of hiPSC spheroids in PGmatrix, showing superior performance and the best maintenance of pluripotency among all existing methods studied in this work such as a PEG-based temperature-sensitive hydrogel

for 3D culture.<sup>[35]</sup> Further, we modified the backbone structure of PGmatrix sequence by increasing its hydrophobic segment to achieve PGmatrix-M with stronger hydrophobic interaction, hence, to obtain tunable gel strength and fast self-healing kinetics in a broad range suitable for either pipetting or 3D bioprinting. The hiPSCs in PGmatrix-M showed a 15–25-fold increase in proliferation with a viability above 95% as well as maintenance of pluripotency.

In particular, we demonstrated that the PGmatrix-M could be printed by extrusion bioprinters into various patterns without requiring additional chemical crosslinking and the printed constructs remained stable in culture medium for up to 3 months. Furthermore, we printed the PGmatrix-M bioink encapsulated with either hiPSCs single cells or spheroids recovered from cell manufacturing using PGmatrix-M as 3D scaffolding. The PGmatrix-M overcomes the scale limitation of U-bottom plates<sup>[15]</sup> or microarray molding techniques<sup>[16]</sup> and enables highly efficient translational investigations. Finally, the unique bioprinting feature of PGmatrix-M is promising for large-scale manufacturing of hiPSC spheroids or somatic cells such as hepatocytes or cardiomyocytes through the differentiation in a stirring tank bioreactor system in the future.

## 2. Results and Discussion

### 2.1. Peptide Hydrogel Possessed Tunable Gel Strength, Shear-Thinning Viscosity, and Self-Healing Properties

The peptide hydrogel (PGmatrix), which is mainly prepared from the h9e peptide,<sup>[30]</sup> was formulated with the commonly used culture medium mTeSR1 for hiPSCs and formed a self-supporting hydrogel (**Figure 1A**). The self-assembling nature of the PGmatrix was observed by measuring gel formation as a function of time. Within a few seconds, the gel strength reached 100 Pa at peptide concentrations of 0.5% and 1.0%, which is sufficient for self-support. The elastic moduli of PGmatrix at 30 min reached 240, 620, and 996 Pa at 1 Hz (Table S1, Supporting Information), corresponding to peptide concentrations of 0.2%, 0.5%, and 1.0%, respectively. For observation of the sol-gel reversible (self-healing) behaviors, the hydrogel samples were sheared into liquid-like solutions with 0.1–0.5 Pa of elastic moduli (**Figure 1B**). As soon as the shear force was removed, the gel quickly started recovering in a few seconds, after 1 min, the gel strength was recovered back to 69%, 73%, and 72% of its original strength corresponding to 0.2%, 0.5%, and 1.0% peptide concentrations, respectively (Table S1, Supporting Information), and all three samples were up to 95% gel strength by 10 min (**Figure 1B**). The hydrogel of PGmatrix presented entangled nanofibers forming a porous nanoweb like scaffolding morphology and a mixture of single nanofibers ( $\approx 20$  nm in diameter) and nanofiber clusters ( $\approx 100$ – $500$  nm in diameter) (**Figure 1C**). A heterogeneous pore size was observed ranging from 500 to 2500 nm at 0.01% peptide concentration (**Figure 1C**).

Although the PGmatrix hydrogel has shown desirable rheological properties for 3D cell culture with superior cell performance,<sup>[34]</sup> it has limited printability. Thus, we modified the PGmatrix hydrogel by elongating the hydrophobic segment

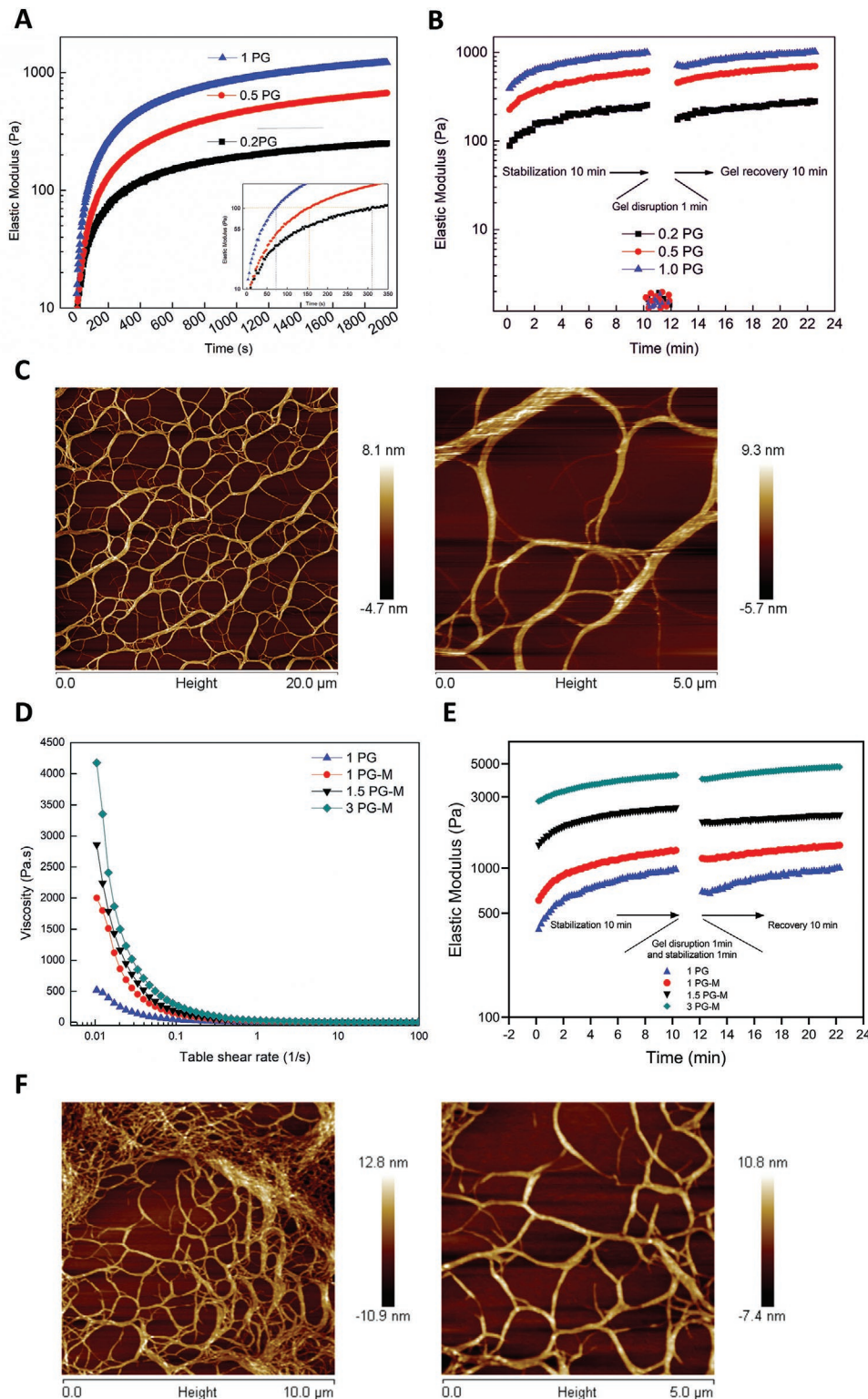


**Figure 1.** Peptide hydrogels (PGmatrix and PGmatrix-M) possessed tunable properties. A) Storage moduli of PGmatrix were directly proportional to the concentrations of peptide nanofibers during the 30 min gelation process at 37 °C. B) Storage moduli of PGmatrix were directly proportional to the concentrations of peptide nanofibers in both shear-thinning and sol-gel recovery tests. Gel strengths were 69%, 73%, and 72% recovered by 1 min after shear force removal at 0.2%, 0.5%, and 1% peptide concentrations, respectively. C) AFM images of the PGmatrix nanostructure at low (left) and high (right) resolutions. D) PGmatrix-M exhibited shear-thinning behaviors at 1%, 1.5%, and 3% peptide concentrations. E) PGmatrix-M was sol-gel-reversible with 87%, 84%, and 94% gel strengths recovered by 1 min after shear force removal at 1%, 1.5%, and 3% peptide concentrations, respectively. F) AFM images of the PGmatrix-M nanostructure at low (left) and high resolution (right).

of the h9e sequence to enhance the hydrophobic interaction, hence, to broaden the gel viscosity, strength, and self-healing kinetics without affecting the cytobiological functions of PGmatrix to obtain a universal peptide hydrogel (PGmatrix-M). The PGmatrix-M presented similar shear-thinning profile as PGmatrix but the initial viscosity increased from 500 to 2000 Pa s at the same peptide concentration (1%) (Figure 1D). The PGmatrix-M possessed large range of tunable gel strength up to 4204 Pa and fast self-healing kinetics from 84% to 94% by 1 min after the shear force was removed (Figure 1E and Table S1, Supporting Information). In addition, because of the increased hydrophobic interaction, the PGmatrix-M presented more heterogeneous morphology with thicker nanofiber bundles and uniform nanoweb structure (Figure 1F), while PGmatrix has more uniform nanoweb structure. The pore size of the PGmatrix-M was from 200 to 1800 nm at 0.01% peptide concentration smaller than that of PGmatrix at the same peptide cementation, as estimated from atomic force microscopy (AFM) images (Figure 1F).

## 2.2. The PGmatrix Hydrogel Showed Superior hiPSC Maintenance Compared to Traditional 2D Methods

To find acceptable culture conditions, we initially examined two hiPSC cell lines grown with the PGmatrix hydrogel at various cell seeding densities from  $1 \times 10^4$  to  $2 \times 10^6$  cells mL $^{-1}$ . hiPSCs from applied stem cell (ASC-hiPSCs) were encapsulated in 3D PGmatrix and fed with mTeSR1 supplemented with Rho-associated protein kinase (ROCK) inhibitor Y-27632. We found that gel strength within the range tested had little effect on hiPSC proliferation and viability (Figure 2A), but a seeding density of  $2 \times 10^5$  cells mL $^{-1}$  resulted in optimal growth performance (Figure 2B,  $p < 0.05$ ). Both ASC-hiPSCs and hiPSCs from Thermo Fisher (TF-hiPSCs) were maintained in the 3D PGmatrix at a 0.5% peptide concentration and  $2 \times 10^5$  cells mL $^{-1}$  seeding density for long-term hiPSC maintenance for up to 37 passages. These two cell lines were also cultured in Matrigel- or vitronectin-XF-coated plates in parallel for comparison purposes because these 2D methods have been considered the gold standard for hiPSC culture. As expected, ASC-hiPSCs in 3D PGmatrix formed small transparent spherical colonies (Figure 2C) and were physiologically expanded in a 3D manner to become spheroids with diameters of  $\approx 20\text{--}50$   $\mu\text{m}$  by day 5, as shown in Figure 2D, while cells formed stretched and flattened monolayer colonies on 2D Matrigel (Figure 2E). The ASC-hiPSCs in a 3D system showed significantly higher fold expansion ( $p = 0.014$ ) and cell viability ( $p < 0.0001$ ) (Figure 2F) than those in 2D Matrigel (Figure 2G). The variance in fold expansion across multiple passages of ASC-hiPSCs was significantly smaller in a 3D system ( $15.70 \pm 3.70$ ) than in a 2D system ( $10.55 \pm 7.05$ ) ( $p < 0.05$ ), which is likely related to different degrees of exposure to the environment. In 2D culture, changes in the environment caused by medium change and routine handling would induce a direct disturbance of homeostasis,<sup>[36]</sup> while hiPSCs in 3D PGmatrix are surrounded by hydrogel, which acts as a protecting cushion that eases potential environmental impacts. Similar results were obtained with the TF-hiPSCs between the 3D and 2D systems ( $p \leq 0.01$ ),

where vitronectin-XF-coated plates were used in the 2D method (Figure S1A–D and Section S2.1, Supporting Information). Fixation and immunostaining of the ASC-hiPSCs grown for 5 d in PGmatrix *in situ* (Figure 3A,B) showed the expression of Oct4 in most cells. Flow cytometry results confirmed the Oct4 expression and further demonstrated high expression levels of Sox2, Nanog, and SSEA4 in the 3D PGmatrix-grown hiPSCs with surprisingly low levels of TRA-1-81 (Figure 3C and Figure S2 and Section S2.2, Supporting Information). However, some studies have suggested that SSEA4 and TRA-1-81 are dispensable for pluripotency.<sup>[37,38]</sup>

To further examine how 3D culture affects the pluripotency of hiPSCs, we performed reverse transcription quantitative polymerase chain reaction (RT-qPCR) analysis on 15 stem cell-related genes using total mRNA extracted from four passages (P7, P10, P15, and P25) of the hiPSCs cultured in 3D PGmatrix and two passages (P10 and P15) of the cells cultured with 2D methods and the pooled results were used for comparison between the 3D and 2D systems. The fold changes in gene expressions were normalized using data from the 2D hiPSCs with the lowest passage number as a reference. In general, the expression levels of NANOG, OCT4, SOX2, DNMT3B, DPPA4, Myc, and ESG1 were not significantly different between the 2D and 3D cultures (Figure 3D for ASC-hiPSCs and Figure S1E for TF-hiPSCs, Section S2.1, Supporting Information). However, the hiPSCs cultured in the 3D PGmatrix exhibited significantly higher expressions of UTF1 and hTERT but lower expression of REX1 than those cultured with 2D methods (Figure 3D and Figure S1E, Supporting Information). UTF1 was suggested as a more sensitive marker than classic Oct4 and NANOG to evaluate stemness<sup>[39]</sup> and was found to play an important role in chromatin formation in embryonic stem cells (ESCs).<sup>[39]</sup> The hTERT transcriptor is critical in maintaining the integrity of telomeres in pluripotent stem cells.<sup>[40]</sup> Overexpression of hTERT in human mesenchymal stem cells (hMSCs) increased the differentiation potential and decreased spontaneous differentiation.<sup>[41]</sup> On the other hand, REX1 (also known as Zfp42) regulates human stem cell pluripotency by maintaining mitochondria in an immature state and stem cells in a highly glycolytic state.<sup>[42]</sup> Though widely used as a pluripotent stem cell marker,<sup>[43]</sup> knockout of REX1 ( $REX1^{-/-}$ ) in ESCs did not seem to affect cell proliferation and pluripotency.<sup>[44,45]</sup> Function of REX1 may be critical to protecting hiPSCs in 2D culture because a high oxygen level in 2D culture triggers mitochondrial oxidative phosphorylation. However, upregulation of REX1 might not be necessary in the 3D peptide hydrogel system because the oxygen level was buffered by hydrogel scaffolding, creating an environment with lower oxygen level that favors human ESC and hMSC maintenance.<sup>[46]</sup>

We also found that the hiPSCs in the 3D PGmatrix had lower or similar expressions of AFP, SOX1, and Brachyury than those in 2D PGmatrix (Figure 3D). These data suggested that the hiPSCs cultured in 3D PGmatrix maintained their pluripotency and undifferentiated status better than their 2D counterparts. Furthermore, the ASC-hiPSCs cultured in the 3D PGmatrix displayed a completely normal karyotype<sup>[47]</sup> up to 37 passages (Figure 3E), suggesting that prolonged culture of hiPSCs in 3D PGmatrix hydrogel did not cause chromosomal abnormalities. Variations in the expression levels of fibroblast

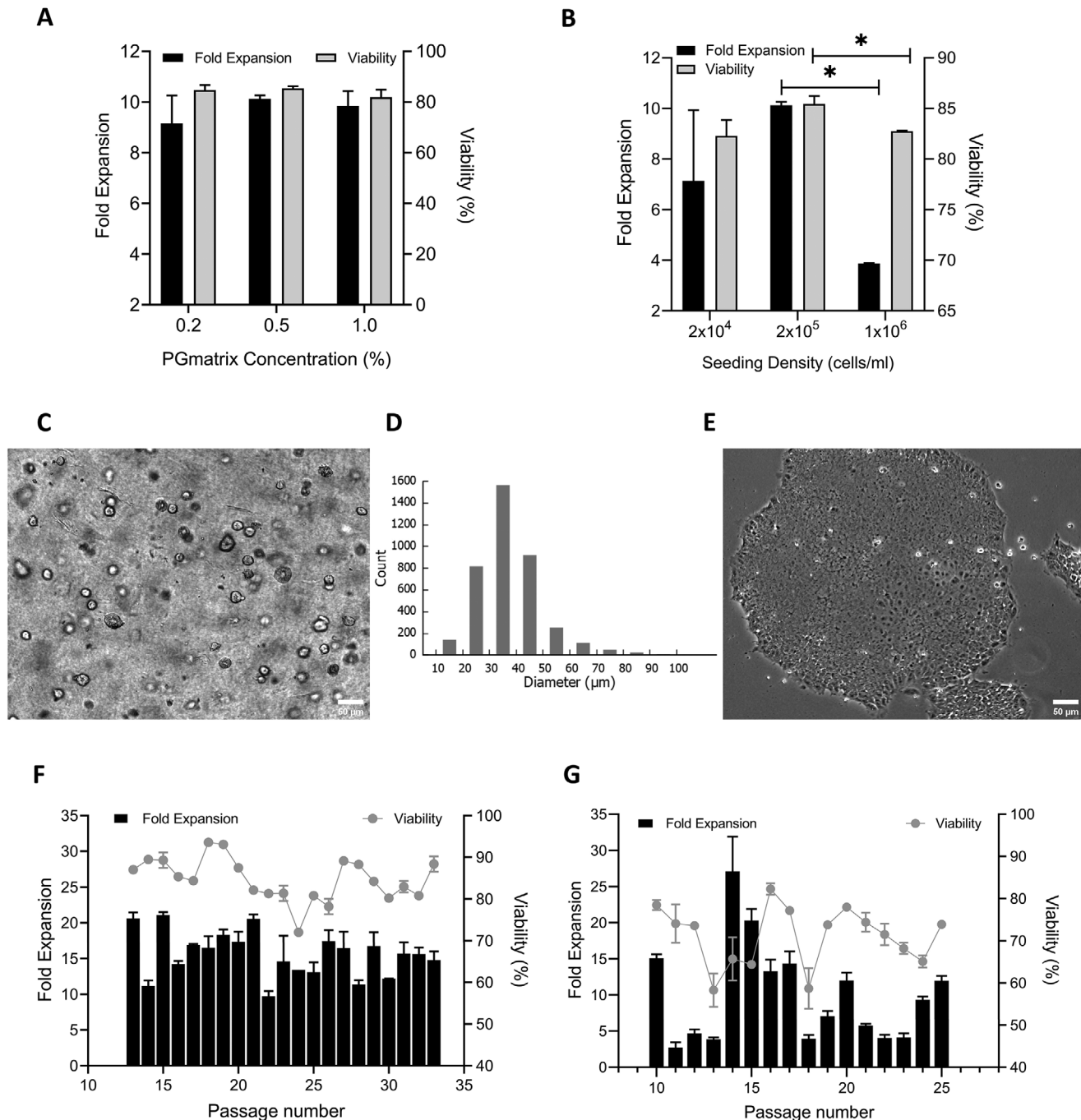


**Figure 2.** The PGmatrix hydrogel showed superior hiPSC maintenance compared to traditional 2D methods. A) No significant differences were found among different concentrations of PGmatrix either in fold expansion or cell viability of ASC-hiPSCs. Fold expansion = number of cells harvested/number of cells seeded. Cell viability is expressed as a percentage of live cells of the total number of cells harvested. Data are shown as means  $\pm$  Standard deviations (SDs). B) Fold expansion and cell viability of the ASC-hiPSCs in 0.5% PGmatrix appeared to be inversely proportional to seeding densities beyond  $2 \times 10^5$  cells  $\text{mL}^{-1}$ . \*:  $p < 0.05$ . C) ASC-hiPSC morphology in 3D PGmatrix. Scale bar, 50  $\mu\text{m}$ . D) Size distribution of the 3D-cultured ASC-hiPSC spheroids harvested from PGmatrix. Data acquired from 24 images of acridine orange (AO)-stained spheroids, with 3900 spheroids counted. E) ASC-hiPSC morphology in 2D on Matrigel. Scale bar, 50  $\mu\text{m}$ . F) The growth performance of the ASC-hiPSCs in 3D PGmatrix remained consistent at a high level through multiple passages up to P34. The overall fold expansion and viability were  $15.70 \pm 3.70$  and  $85.6 \pm 5.70$ , respectively. Data are shown as means  $\pm$  SDs. G) Growth performance of the ASC-hiPSCs cultured on 2D Matrigel fluctuated dramatically through multiple passages compared to those in 3D PGmatrix. The overall fold expansion and cell viability were  $10.55 \pm 7.05$  and  $70.10 \pm 7.49$ , respectively. Data are shown as mean  $\pm$  SD.

growth factor 4 (*FGF4*) and growth differentiation factor 3 (*GDF3*) observed between these two cell lines (ASC-hiPSCs

and TF-hiPSCs) might be related to the different tissue origins from which the two hiPSCs were derived (Figure 3D and

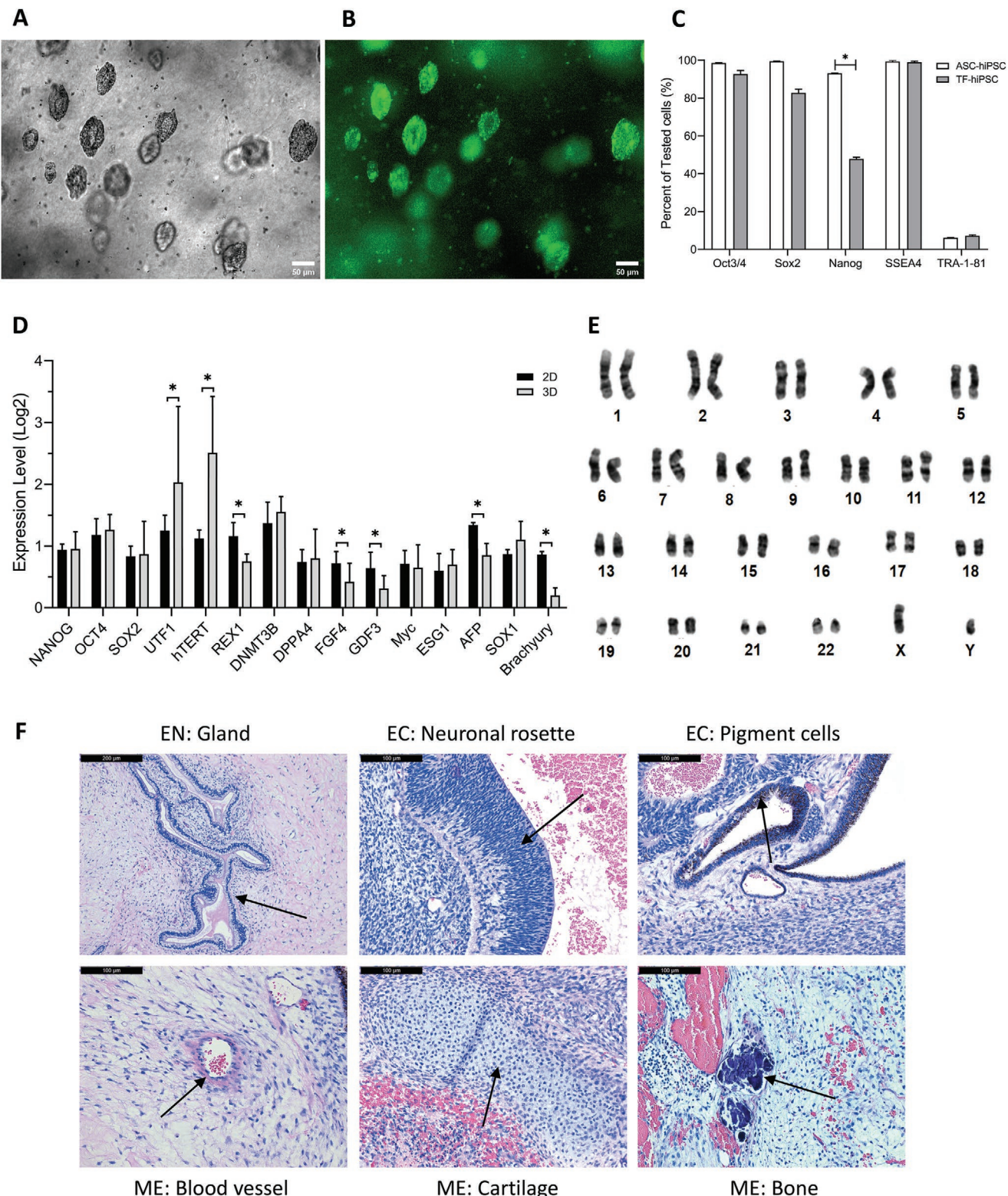


**Figure 3.** ASC-hiPSCs maintained pluripotency during long-term culture in 3D PGmatrix hydrogel. A,B) The ASC-hiPSCs cultured in 3D PGmatrix were fixed and stained with Alexa Fluor-488 s antibody for Oct4 *in situ*. A) Representative brightfield images and B) fluorescence images are shown. Scale bar, 50  $\mu$ m. C) Flow cytometric analysis of two hiPSC lines cultured in 3D PGmatrix demonstrated high expression of Oct3/4, SOX2, NANOG, and SSEA4 but low expression of TRA-1–81. Data are shown as means  $\pm$  SDs. \*:  $p < 0.05$ . D) ASC-hiPSCs showed upregulation of pluripotency-related genes in 3D PGmatrix. 2D results were averaged from two different passages (P10 and P15), while 3D results were averaged from four different passages (P7, P10, P15, and P25). Expression levels were calculated using the results from the lowest 2D passage (P10) as a reference. Data are shown as means  $\pm$  SDs. \*:

Figure S1E, Supporting Information). A teratoma assay indicated differentiation into three germ layers in vivo, suggesting that the ASC-hiPSCs maintained their pluripotency after long-term 3D culture in PGmatrix (Figure 3F). This also indicated the pluripotent integrity of the 3D-cultured hiPSCs despite the low levels of TRA-1-81, raising the possibility that some of the pluripotent stem cell markers established in 2D culture may need to be revised for the characterization of 3D-cultured hiPSCs. In addition, we demonstrated that cryopreserved ASC-hiPSCs directly cultured in 3D PGmatrix after thawing proliferated well; thus, the 2D method could be omitted (Figure S3 and Section S2.3, Supporting Information) to simplify the workflow of the hiPSC 3D culture as needed.

### 2.3. hiPSCs in the 3D PGmatrix Hydrogel Showed Better Properties than Those in the 3D PEG-Based Hydrogel

PEG-derived hydrogels are considered one of the most popular hydrogels for 3D hiPSC culture. Mebiol gel is a commercial PEG-based hydrogel whose gelation is triggered by a temperature increase from ice-cold to physiological.<sup>[35]</sup> It also provides hypoxic conditions that may favor 3D culture of hiPSCs. We examined the phenotypes and pluripotency of hiPSCs in 3D Mebiol gel and 3D PGmatrix using ASC-hiPSCs in either mTeSR1 or E8 medium supplemented with the ROCK inhibitor Y-27632 to yield four culture conditions (PG-mT, PG-E8, Mebiol-mT, and Mebiol-E8). Under the best conditions (PG-mT vs Mebiol-E8), the fold expansion ( $13.96 \pm 1.87$ ) and cell viability ( $84.2 \pm 2.0\%$ ) of the hiPSCs cultured in PGmatrix were significantly higher than those cultured in Mebiol gel (fold expansion  $9.69 \pm 2.38$ , viability  $13.0 \pm 1.6\%$ ) (Figure 4A). The fold expansion of the PG-mT group was significantly higher than that of the PG-E8 group, but the fold expansion of the PG-E8 group increased as the peptide concentration was decreased from 0.5% to 0.3% (Figure 4A).

In 3D PGmatrix with either mTeSR1 or E8 culture medium, hiPSCs showed more uniform spherical morphology than those in Mebiol gel (Figure 4B and Figure S4A and Section S2.4, Supporting Information). In 3D Mebiol gel, hiPSCs formed a few large spheroids in E8 medium, and the cells on the edge of the large spheroids seemed to be dying (Figure 4B). Notably, in mTeSR1 medium, much smaller spheres and much lower fold expansion were observed in Mebiol gel (Figure S4A, Supporting Information) than those in the Mebiol-E8 group (Figure 4A and Figure S4B and Section S2.4, Supporting Information). Although the fold expansion was stable at approximately tenfold during several Mebiol-E8 hiPSC culture experiments, consistent with a previous report,<sup>[35]</sup> the viability was no more than 20% regardless of which medium (E8 or mTeSR1) was used (Figure 4A and Figure S4B, Supporting Information). As a result, we were not able to compare 3D culture of Mebiol gel with PGmatrix for long-term performance.

Next, we examined the pluripotency of the hiPSC spheroids formed in 3D PGmatrix and 3D Mebiol gel using ASC-hiPSCs with the better culture conditions (Mebiol-E8 and PG-mT). As shown in Figure 4C, hiPSC gene integrity was well maintained in the 3D PGmatrix compared to that in the 3D Mebiol gel. hiPSC spheroids grown in 3D PGmatrix expressed higher levels of pluripotent markers (*NANOG*, *OCT4*, *SOX2*, and *hTERT*) and lower or similar expressions of differentiation markers (*AFP*, *SOX1*, and *Brachyury*) than those grown in 3D Mebiol gel. Likewise, the expression levels of *REX1*, *DNMT3B*, and *FGF4* were also significantly reduced in the hiPSCs grown in Mebiol-E8. This implies that hiPSCs grown in Mebiol-E8 were more likely to unwanted differentiate since *DNMT3B* is responsible for de novo DNA methylation.<sup>[48]</sup> These results indicated that spheroids formed in the 3D PEG-based hydrogel had lower pluripotency than those in the 3D PGmatrix. In addition, hiPSC spheroids formed in suspension with nonadherent U-bottom 96-well plates using 2D-cultured ASC-hiPSCs<sup>[15]</sup> were also included for comparison (Figure 4C). We observed strong upregulation of *SOX1* and *Brachyury* and downregulation of *NANOG*, *OCT4*, *SOX2*, *hTERT*, and *Myc*, indicating initiation of unwanted differentiation in the hiPSC spheroids formed by the U-bottom suspension method. This finding suggested that the suspension method may be used to initiate differentiation but is not suited for the maintenance of hiPSC integrity.

To investigate the variations between PGmatrix and Mebiol gel in either mTeSR1 or E8 medium (Figure 4A), we examined the gel strength kinetics of PGmatrix as a function of culture time in ASC-hiPSCs. Interestingly, the decrease in gel strength during cell culture (Figure 4D i) seemed inversely related to spheroid growth performance (Figure 4A). The gel strength for 0.5% PGmatrix-mTeSR1 (0.5PG-mT) decreased the most rapidly, leading to the highest fold-expansion and viability. However, the 0.5% PGmatrix-E8 (0.5PG-E8) group had the lowest reduction in gel strength with the lowest fold expansion and viability. While the gel strength, by soaking the gel alone without cells in these culture media, remained the same in E8 and decreased gradually in mTeSR1 (Figure 4D ii). This finding suggested that gel degradability may affect 3D spheroid growth performance.

There are many cues to determine cell fate, and among those, physical cues, chemical cues, and biological cues have been highly recognized. Cell-environment interactions have been proven to be an important physical cue for 3D culture. Stem cells secrete various substances during their growth, such as proteases and ECM proteins.<sup>[49–51]</sup> The Hippo pathway has attracted increased attention as researchers attempt to elucidate the role of mechanical cues in stem cell niches. Mechanosensing genes Yes-associated protein 1 (YAP) and transcriptional coactivator with PDZ-binding motif (TAZ)<sup>[52,53]</sup> are at the center of this signaling cascade. Therefore, we determined the expression levels of YAP and TAZ in the hiPSCs cultured in several 3D culture conditions (Figure 4E). We found that the YAP/TAZ expression levels did not differ between 0.5% and

*p* < 0.05. E) ASC-hiPSCs showed a normal male karyotype after long-term 3D culture in PGmatrix. F) The ASC-hiPSCs collected from 3D PGmatrix at a high passage (P34) were injected into immunodeficient mice to induce teratoma formation. Representative tissues for each of the three germ layers, endoderm (EN), ectoderm (EC), and mesoderm (ME), are presented.

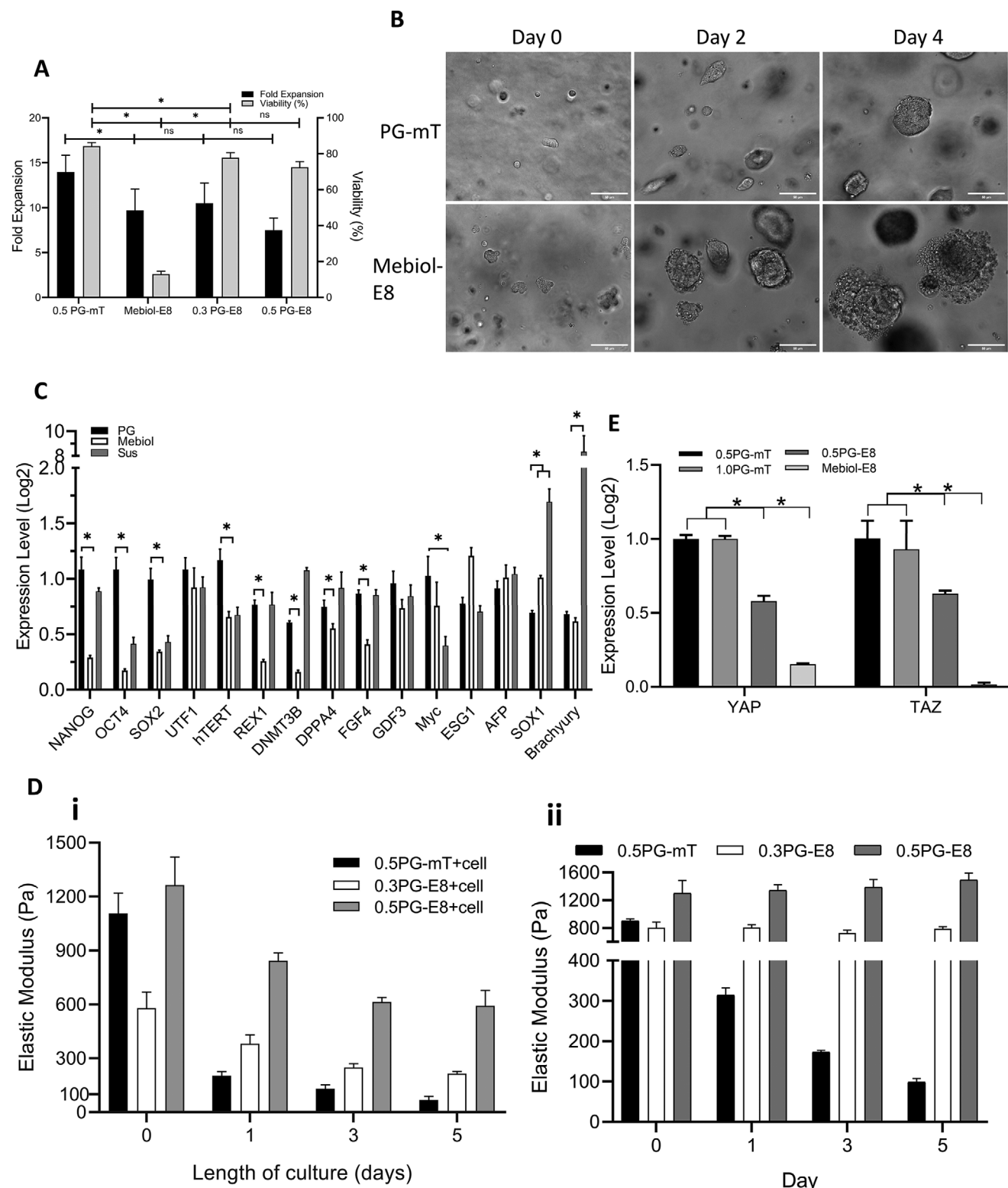
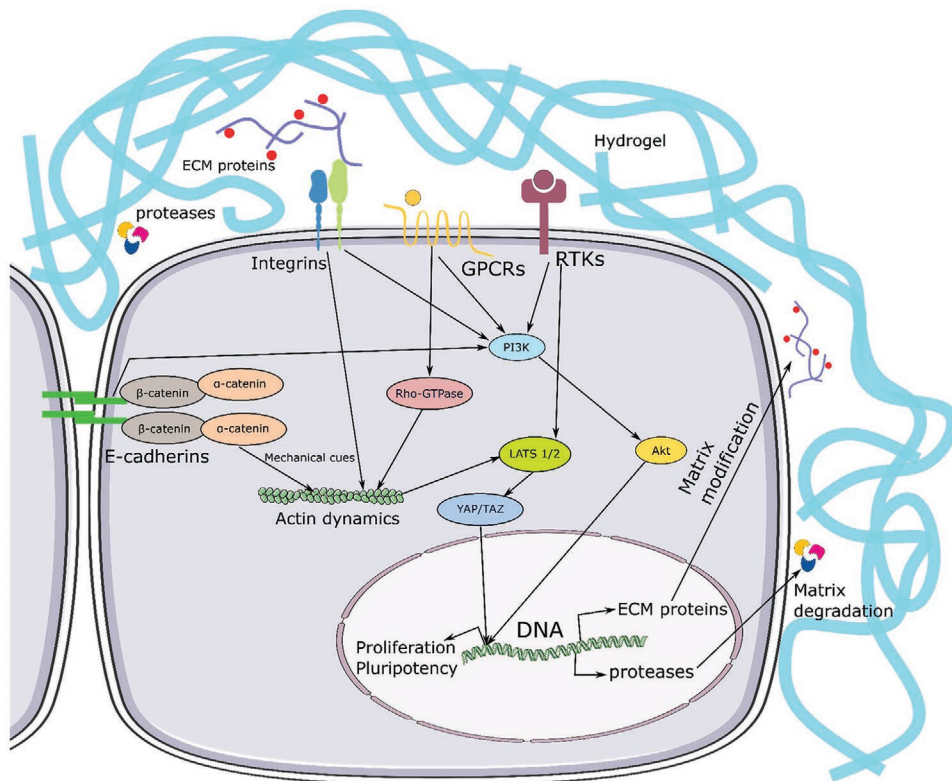


**Figure 4.** hiPSCs in the 3D PGmatrix hydrogel showed superior properties compared to those in the 3D PEG-based hydrogel. A) ASC-hiPSCs grew better in 3D PGmatrix (0.5%) with mTESR1 (0.5 PG-mT) than in 3D Mebiol gel with E8 medium (Mebiol-E8). With E8 medium, ASC-hiPSCs grew better in 3D PGmatrix at lower peptide concentrations (0.3%) (0.3 PG-E8) than in 3D PGmatrix at higher peptide concentrations (0.5%) (0.5 PG-E8). During harvesting, every two wells were pooled and one sample from each pool was taken in triplicate for cell counting and viability assays. Data are shown as means  $\pm$  SDs. \*:  $p < 0.05$ . B) Morphology of hiPSCs grown in PG-mT and Mebiol-E8 on days 0, 2, and 4 after encapsulation. Scale bar, 50  $\mu$ m. C) Pluripotency-related gene expression of ASC-hiPSCs from 3D PGmatrix with mTeSR1 (PG), 3D Mebiol gel with E8 (Mebiol), and suspension



**Scheme 1.** Proposed mechanism for hiPSC growth and maintenance of pluripotency in 3D PGmatrix hydrogel. Cells actively modify the surrounding 3D microenvironment by secreting proteases as matrix-degrading enzymes and ECM proteins. These modifications facilitate cell migration and signaling via cell-cell contact (E-cadherin) and paracrine signaling molecules. In addition to soluble factor signaling, physical (mechanical strength) cues from the cell-matrix or cell-cell adhesions affect the actin-myosin cytoskeleton and send signals via the Hippo pathway, eventually affecting the expression of mechanosensitive YAP/TAZ genes to regulate and sustain proliferation and pluripotency in hiPSCs to achieve long-term hiPSC maintenance. GPCRs—G protein-coupled receptors and RTKs—receptor tyrosine kinases.

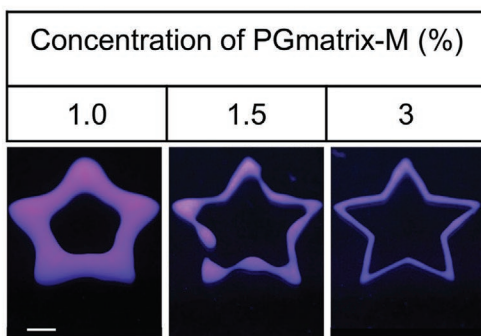
1% PGmatrix with mTeSR1 but decreased significantly in the hiPSCs grown in 0.5% PGmatrix with E8 and in Mebiol gel with E8 medium (Figure 4E). The different expression levels were inversely related to the degradability of the gel, thus suggesting that the expression of YAP/TAZ was linked to gel degradability. Thus, the low fold expansion and viability observed with the hiPSCs grown in Mebiol gel is likely the result of a nondegradable microenvironment (Figure 4A, 4E). In addition, we preliminarily examined if there was any functional component in PGmatrix would interact with hiPSCs by culturing hiPSCs on 2D with PGmatrix coating. We observed strong hiPSC agglomeration, suggesting that there was no cell attachment (Figure S5A and Section S2.5, Supporting Information). With addition of vitronectin, an ECM protein containing hiPSC binding sites, to PGmatrix coating, we observed hiPSC morphology similar to those in 2D culture with Matrigel (Figure S5B and Section S2.5, Supporting Information). However, when the PGmatrix-vitronectin was used for 3D hiPSC culture, the cell

colonies started losing their spherical shape (Figure S5C, Supporting Information) and become worse as percentage of vitronectin increased (Figure S5D and Section S2.5, Supporting Information). These results suggest that PGmatrix would not directly bind to hiPSCs to support their growth.

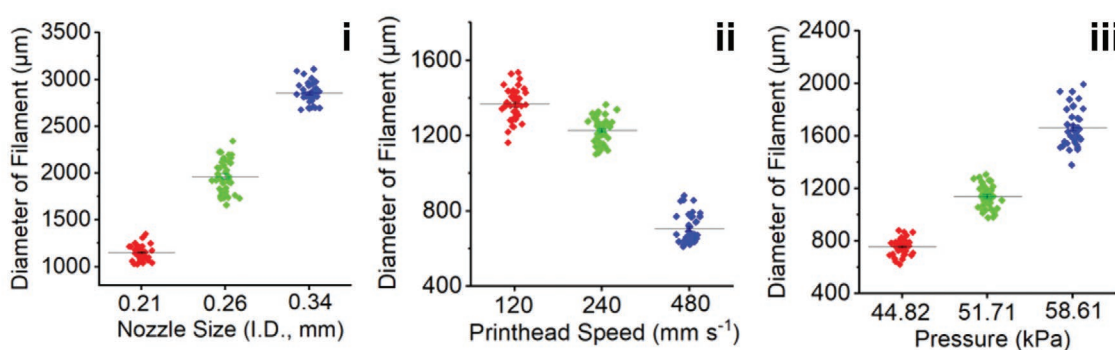
We speculated that when encapsulated in a 3D matrix, factors from the culture medium and secreted by hiPSCs may continually modify the surrounding environment to favor cell proliferation and pluripotency maintenance. As illustrated in Scheme 1, initially following the encapsulation of sufficient number of hiPSCs, some soluble factors such as insulin, bFGF, TGF $\beta$ , and Nodal from medium supplement would bind to surface receptors such as GPCRs (G protein-coupled receptors) and RTKs (receptor tyrosine kinases) to activate essential pathways including phosphoinositide-3-kinase–protein kinase B/Akt (PI3K/Akt) for survival.<sup>[54]</sup> PI3K/Akt responding to signaling from adhesion and binding of various surface receptors with soluble factors has been proven essential for pluripotent stem

spheroids from nonadherent U-bottom plates (Sus). Data from each passage were obtained in triplicate and from three separate experiments. ASC-hiPSCs harvested immediately before parallel culture were used as controls. Data are shown as means  $\pm$  SDs. \*:  $p < 0.05$ . D) Changes in gel elastic modulus in PGmatrix during a 5 d culture period in mTeSR1 and E8 culture media at various peptide concentrations i) with and ii) without ASC-hiPSC encapsulation. Data are shown as means  $\pm$  SDs. E) Expression of YAP/TAZ in the hiPSCs grown under different 3D culture conditions. Data are shown as means  $\pm$  SDs. \*:  $p < 0.05$ .

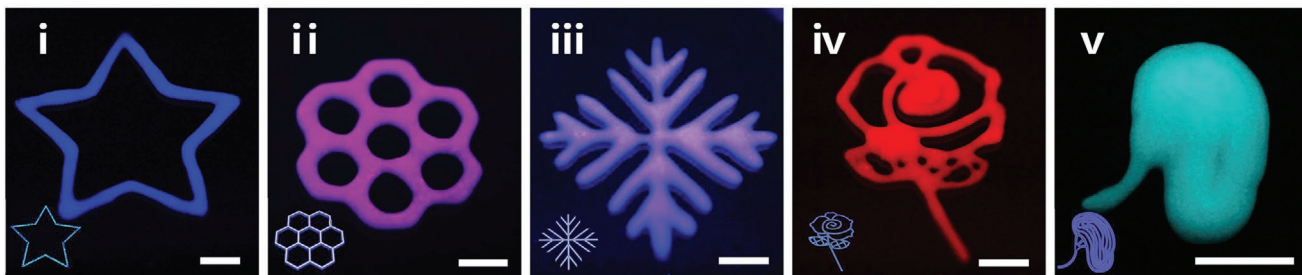
**A**



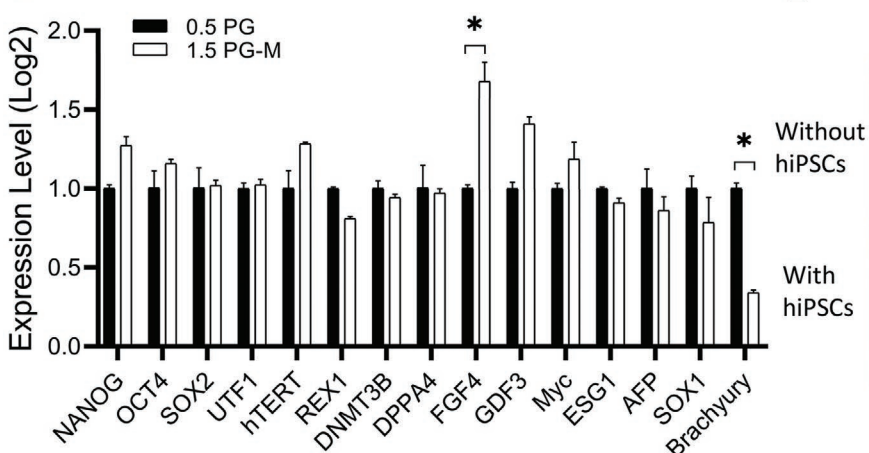
**B**



**C**



**D**



**E**

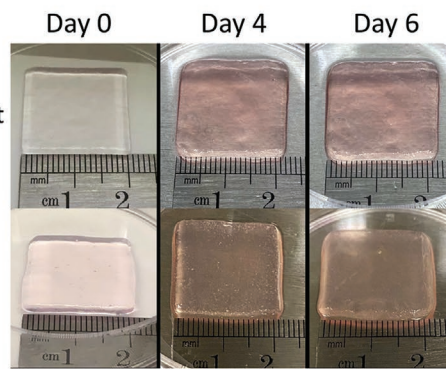


**Figure 5.** Printability and hiPSCs performance of PGmatrix-M as bioink. A) Printing resolution of PGmatrix-M at different concentrations. Scale bar, 5 mm. B) Effects of i) nozzle size, ii) printhead moving speed, and iii) printing pressure on the printability of PGmatrix-M bioink. C) Bioprinted PGmatrix-M constructs (3%) of different patterns. Scale bar, 5 mm. D) ASC-hiPSCs cultured in 1.5% PGmatrix-M (1.5 PG-M) did not exhibit major expression pattern differences in pluripotency related genes compared to those cultured in 0.5% PGmatrix (0.5 PG). Data are shown as mean  $\pm$  SD. \*:  $p < 0.05$ . E) The PGmatrix-M construct remained stable for at least 6 d with or without hiPSCs (constructs were disrupted for cell harvesting for further analysis by day 6).

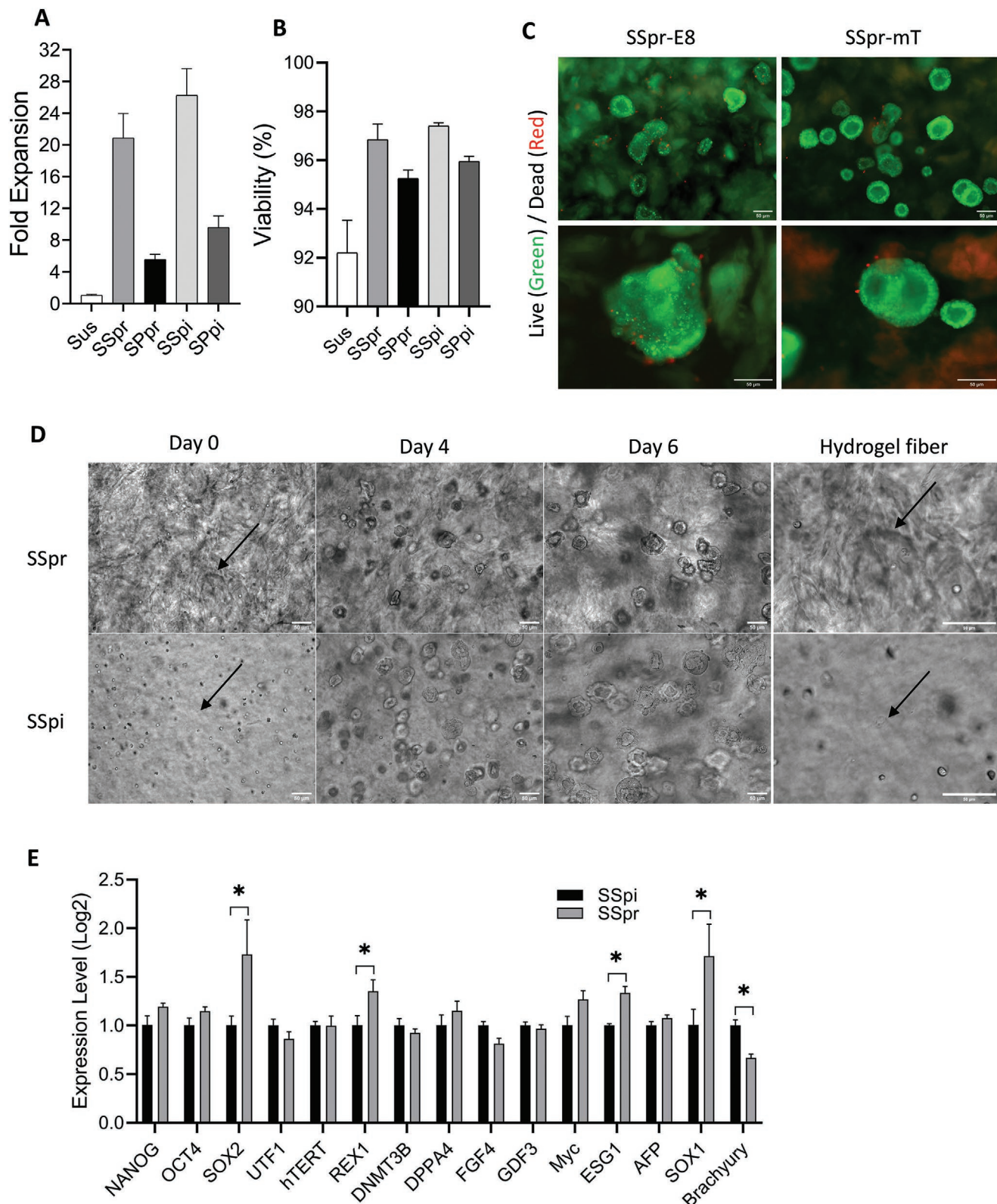


**Figure 6.** The bioprinting process did not substantially affect the growth performance of ASC-hiPSCs encapsulated in PGmatrix-M bioink hydrogel. A) Fold expansion and B) viability of the ASC-hiPSCs under different conditions: suspension spheroids (Sus) using the nonadherent U-bottom 96-well plate method, single cells printed and grown into spheroids (SSpr), single cells pipetted and grown into spheroids (SSpi), spheroids printed and continued growing as spheroids (SPPr), and spheroids pipetted and continued growing into spheroids (SPpi). Data are shown as means  $\pm$  SDs.

cell maintenance.<sup>[55–61]</sup> During this initial survival and adaptation period, hiPSCs would initiate their secretion of ECM proteins and some proteases that would start remodeling the surrounding PGmatrix environment through matrix degradation and modification. Meanwhile, the secreted ECM proteins such as laminin and vitronectin would bind to integrin that would trigger various related signaling pathways to promote proliferation and pluripotency maintenance.<sup>[50,62,63]</sup> The microenvironment of ECM-protein-modified-PGmatrix would facilitate cell migration, leading to increased cell-cell contact via E-cadherin.<sup>[64–66]</sup> Cell-ECM protein signaling via integrin and cell-cell signaling via E-cadherin are closely linked to cell cytoskeleton, these binding events occurred at cell surface would affect actin dynamics and relay the signals through Hippo pathway. With appropriate mechanical signals, the signaling cascade including large tumor suppressor kinase 1/2 would cause upregulation of the mechanosensitive YAP and TAZ proteins, as observed in the RT-qPCR analysis (Figure 4E). These YAP/TAZ proteins would then relocate into the nucleus to affect gene expression related to pluripotency maintenance.<sup>[67–72]</sup> Critical maintenance pathways including PI3K/Akt can be enhanced by cells through “remodeling” of their microenvironment. Soluble signaling factors such as bFGF and TGF $\beta$  are also part of hiPSC secretome that would contribute to hiPSC maintenance through paracrine signaling. Therefore, the degradability or modifiability of a 3D matrix should be a critical property influencing hiPSC growth performance and maintenance of pluripotency, which has been proven true for neural progenitor cells.<sup>[52]</sup> It would be integrating to further confirm the role of PGmatrix in Hippo signaling pathway.

As shown in Figure S5A in the Supporting Information, we did not observe any obvious physical attachment function of the PGmatrix to hiPSCs; however, it is not necessary to assume PGmatrix would not contain any unique functions contributing to chemical or biological cues. The PGmatrix sequence was inspired from the calcium binding motif of the human muscle protein and the  $\beta$ -spiral motif of the spider flagelliform silk protein.<sup>[30,31]</sup> Whether any or both two protein domains are unique contributors to 3D culture of iPSCs is worthy to be systematically and thoroughly investigated, which would be valuable information for future design and fabrication of functional materials for iPSCs or other stem cells.

#### 2.4. hiPSCs Showed High Survivability and Superior Performance in 3D Bioprinting with Universal Peptide Hydrogel Bioink

Printability was first examined by extruding the PGmatrix-M bioink at different concentrations (1.0%, 1.5%, and 3.0%). While the star pattern had a thicker lining at 1.0%, the resolution was improved when the concentrations were elevated to 1.5% and 3.0% (Figure 5A). In all cases though, the PGmatrix-M bioink

self-healed back to the gel without any postprinting crosslinking aids from neither light (e.g., UV) nor chemicals or ions. The effects of extrusion conditions were examined by evaluating the influences of nozzle size (Figure 5B i), printhead moving speed (Figure 5B ii), and printing pressure (Figure 5B iii) on the diameter of filaments, using the 3.0% PGmatrix-M bioink. The printing versatility was evaluated using the same bioink by producing patterns from a simple star to a rose and to a kidney shape, featuring various levels of complexity (Figure 5C).

Furthermore, the hiPSCs formed physiological spheroids and were highly proliferated with viability above 95% in all PGmatrix-M bioinks by pipetting in 3D well-plate culture (Figure S6A and Section S2.6, Supporting Information) and also showed similar morphology and pluripotency compared to PGmatrix at gene expression levels (Figures 2C and 5D). Then, we examined the printability of PGmatrix-M with hiPSCs using an extrusion bioprinter. As reported in the literature, shorter nozzles and low printing pressures generally cause less damage to hiPSCs;<sup>[28]</sup> thus, we chose a cone-shaped nozzle with a 2 mm nozzle channel length and 250  $\mu\text{m}$  inner diameter. Three-layered 20  $\times$  20  $\times$  0.75 mm<sup>3</sup>-sheet constructs with or without hiPSCs were printed at 600 mm min<sup>-1</sup> (29.4  $\mu\text{L}$  min<sup>-1</sup>) and 3–5 kPa gas pressure. The printed construct shapes were stable in culture medium for at least 7 d (Figure 5E), and up to 3 months (Figure S6B and Section S2.6, Supporting Information). With hiPSC loading at a cell density of (2–3)  $\times$  10<sup>5</sup> cells mL<sup>-1</sup>, the actual dimensions in X and Y directions were about 21 mm  $\times$  21 mm, and expanded by 2.5% during 6-d culture, mainly caused by cell growth and cell-induced gel degradation, which can be considered 4D postdevelopment.

For observation of the impact of extrusion bioprinting on hiPSC growth performance and quality, the bioink encapsulated with hiPSC single cells (SS) or spheroids (SP) was plated into 24-well plates by either extrusion bioprinting (pr) or pipetting (pi) and cultured in parallel. The survival rate of hiPSCs after printing was 96.57%, and hiPSC viability was 94.20% and 95.85% at 0 and 24 h after printing, respectively (Figure S6C and Section S2.6, Supporting Information). Cells showed an  $\approx$ 20-fold increase in proliferation by day 6 at 96.9% viability, which was notably higher than suspension spheroids (Sus) harvested from nonadherent U-bottom plates (Figure 6A,B). The printed (SSpr-mT and SSpr-E8) hiPSCs formed similar spheroids in either mTeSR1 or E8 culture media (Figure 6C). The printed (SSpr) and pipetted (SSpi) hiPSCs also formed spheroids with similar morphology (Figure 6D), although the bioprinted constructs presented a rough and oriented fiber bundle-like morphology compared to the pipetted ones with smooth and randomly distributed fibers (Figure 6D arrows). The growth rate of the printed hiPSCs was slower (or delayed by  $\approx$ 24 h) than that of the pipetted hiPSCs, which might be caused by the printing pressure and orientation of hydrogel fibers through the printing nozzle.

C) Spheroids of ASC-hiPSCs grown in E8 or mTeSR1 (mT) harvested from printed single cell samples (SSpr) were stained with viability dyes for live (AO, green) and dead (PI, red) cells. Scale bar, 50  $\mu\text{m}$ . D) Morphological images of ASC-hiPSCs in PGmatrix-M bioink hydrogel and hydrogel fibers (red arrows) in SSpr and SSpi samples. Scale bar, 50  $\mu\text{m}$ . E) The printing process did not strongly affect pluripotency-related gene expression in ASC-hiPSCs. One duplicate sample of SSpi-mT used as a control. Data are shown as means  $\pm$  SDs. \*:  $p < 0.05$ .

3D bioprinting technology has been explored as a solution to meet rapidly growing demands on hiPSCs in the arena of disease modeling, drug screening, cell therapeutics, and regenerative medicines,<sup>[29,73]</sup> but printable biomaterials suitable for hiPSCs are still limited. The precursor solutions would form hydrogels before or after bioprinting via the following processes: 1) photopolymerization: PEG diacrylate,<sup>[20,21]</sup> gelatin methacryloyl (GelMA),<sup>[23,74,75]</sup> and methacrylated hyaluronic acid (MeHA);<sup>[22,75]</sup> 2) ionic crosslinking: alginate,<sup>[26,75]</sup> nanofibrillated cellulose with alginate or hyaluronic acid,<sup>[76,77]</sup> alginate with fibrinogen,<sup>[78]</sup> and peptide based hydrogel;<sup>[79]</sup> 3) a combination of ionic crosslinking reagent and photopolymerization (bisphosphonate-derivatized hyaluronic acid,<sup>[24]</sup> thiolated hyaluronic acid and gelatin<sup>[25]</sup>); 4) temperature control: gelatin-based hydrogel<sup>[23,26,27]</sup> and hydroxypropyl chitin (HPCH) in combination with Matrigel.<sup>[28]</sup> Case studies in the past few years have demonstrated possible 3D bioprinting of hiPSCs for cell aggregate expansion using synthetic thermal-sensitive HPCH and Matrigel<sup>[28]</sup> and for postprinting differentiation into cartilage using nanofibrillated cellulose with alginate or hyaluronic acid,<sup>[77]</sup> into hepatocytes using alginate through valve dispensing with calcium ions as gelation triggers,<sup>[80]</sup> or into neural tissues using alginate with fibrinogen crosslinked with genipin and calcium ions.<sup>[78]</sup> Cell integrity in terms of pluripotency is still limited to a few biomarkers, such as Oct4, NANOG, Sox2, and SSEA4.<sup>[28,81]</sup> In most cases, cell viability is below 40% with pluripotency markers similar or lower than those of 2D or suspension control samples, which can result from printing damage, UV light, overdosage of metal ions or the scaffold itself or a combination of these factors. Thus, the cell loading density for bioprinting is usually high ( $\approx 10^6\text{--}10^8 \text{ cells mL}^{-1}$ ) in these case studies to ensure that enough live cells survive the bioprinting process, which also requires labor-intensive cell preparation before bioprinting.

The PGmatrix-M hydrogel could be an advanced approach to produce high-quality hiPSCs (single cells or spheroids) by either pipetting or bioprinting. This platform can be readily incorporated not only in a regular laboratory but also to high-throughput drug screening and toxicity testing as well as to tank-like bioreactor system for large scale cell manufacturing. With a  $(1\text{--}3) \times 10^5 \text{ cells mL}^{-1}$  loading density in 0.5–1.5% PGmatrix-M,  $\approx 40\ 000\text{--}60\ 000$  spheroids were biologically generated with 95–97% viability, while only 96 spheroids (3000 cells per well) were made with 92% viability using one 96-well U-bottom plate (Figure 6A,B). In addition, the pluripotent status of hiPSC spheroids formed in the PGmatrix-M bioink was not deteriorated by 3D bioprinting (SSpr) compared to pipetting (SSpi) (Figure 6E).

### 3. Conclusion

Optimal 3D culture conditions and tunable universal peptide hydrogel (PGmatrix-M) for high-efficient physiological formation of hiPSC spheroids were developed with consistent cell growth (15–25-fold) and high cell viability above 95% and stable genetic integrity. hiPSCs growth performance is significantly independent of mechanical (i.e., strength and viscosity) and

morphological (i.e., pore size) properties of PGmatrix or PGmatrix-M in the tested ranges. Both PGmatrix and PGmatrix-M are superior scaffolding hydrogel for self-renewing cells such as hiPSCs 3D culture (single cells or spheroids) and long-term maintenance; however, PGmatrix-M demonstrated large scale gel strength, high viscosity, and fast self-healing kinetics suitable for physiological formation of hiPSCs spheroids by either pipetting or bioprinting without the need for photo-, chemical, or ionic crosslinking agents. The hiPSC survival rate was 96% immediately after extrusion bioprinting and the cell viability was above 94% at 0 and 24 h, which suggested that PGmatrix-M provides maximal protection for hiPSCs during printing. PGmatrix-M has potential for hiPSCs for either single-cells or spheroids manufacturing at the industrial scale for downstream applications. Our study demonstrated that the gel degradability by cells strongly favors hiPSC growth performance and this relationship is speculated to link to the Hippo signaling pathway and the mechanosensitive YAP/TAZ pathway. Whether the peptide hydrogel either PGmatrix or PGmatrix-M provides chemical or biological cues that would also attribute to hiPSC growth remains to be investigated.

### 4. Experimental Section

Experimental details are provided in the Supporting Information.

### Supporting Information

Supporting Information is available from the Wiley Online Library or from the author.

### Acknowledgements

The authors sincerely thank the Flow Cytometry Laboratory at the College of Veterinary Medicine, Kansas State University (KSU), for assisting with the flow cytometry analysis. X.S.S. acknowledges the support by the KSU and KSU-Agricultural Experiment Station contribution number is 19-212-J. Y.S.Z. acknowledges the support by the Brigham Research Institute.

### Conflict of Interest

The authors declare no conflict of interest.

### Author Contribution

Q.L. and G.Q. contributed equally to this work. Q.L. and G.Q. performed the hiPSC cultures, flow cytometric assays, immunochemical experiments, and image and data analysis, prepared the peptide hydrogel and bioink, characterized gel and bioink, and contributed to the discussions. X.L. and J.B. designed the primers and performed the RT-qPCR experiments. G.Q., J.Z., G.T., Y.S.Z., M.Z., and D.W. contributed to the 3D bioprinting. R.C.-T. completed the *in vivo* teratoma assays. A.A., J.-Q.H., R.C.-T., Y.S.Z., and Y.Y.Z. provided experimental guidance, contributed to the discussions, and manuscript revision. X.S.S. provided guidance, planned and directed the work and led the discussions. Q.L., G.Q., and X.S.S. conducted literature review and wrote the manuscript.

## Data Availability Statement

The data that support the findings of this study are available from the corresponding author upon reasonable request.

## Keywords

3D culture, bioprinting, gel degradability, hiPSC physiological spheroids, self-healing hydrogels

Received: April 29, 2021

Revised: July 5, 2021

Published online:

- [1] Z. Zhu, D. Huangfu, *Development* **2013**, *140*, 705.
- [2] Y. Kim, Y. A. Rim, H. Yi, N. Park, S. H. Park, J. H. Ju, *Stem Cells Int.* **2016**, *2016*, 1329459.
- [3] D. A. Conner, *Curr. Protoc. Mol. Biol.* **2001**, Chap. 23, Unit 23.2.
- [4] T. Miyazaki, S. Futaki, H. Suemori, Y. Taniguchi, M. Yamada, M. Kawasaki, M. Hayashi, H. Kurnagai, N. Nakatsuji, K. Sekiguchi, E. Kawase, *Nat. Commun.* **2012**, *3*, 1236.
- [5] C. Xu, M. S. Inokuma, J. Denham, K. Golds, P. Kundu, J. D. Gold, M. K. Carpenter, *Nat. Biotechnol.* **2001**, *19*, 971.
- [6] M. Nagaoka, K. Si-Tayeb, T. Akaike, S. A. Duncan, *BMC Dev. Biol.* **2010**, *10*, 60.
- [7] S. Rodin, L. Antonsson, C. Niaudet, O. E. Simonson, E. Salmela, E. M. Hansson, A. Domogatskaya, Z. Xiao, P. Damdimopoulos, M. Sheikhi, J. Inzunza, A.-S. Nilsson, D. Baker, R. Kuiper, Y. Sun, E. Blennow, M. Nordenskjöld, K.-H. Grinnemo, J. Kere, C. Betsholtz, O. Hovatta, K. Tryggvason, *Nat. Commun.* **2014**, *5*, 3195.
- [8] S. R. Braam, L. Zeinstra, S. Litjens, D. W. Oostwaard, S. van den Brink, L. van Laake, F. Lebrin, P. Kats, R. Hochstenbach, R. Passier, A. Sonnenberg, C. L. Mummery, *Stem Cells* **2008**, *26*, 2257.
- [9] M. Nakagawa, Y. Taniguchi, S. Senda, N. Takizawa, T. Ichisaka, K. Asano, A. Morizane, D. Doi, J. Takahashi, M. Nishizawa, Y. Yoshida, T. Toyoda, K. Osafune, K. Sekiguchi, S. Yamanaka, *Sci. Rep.* **2014**, *4*, 3594.
- [10] L. G. Villa-Diaz, H. Nandivada, J. Ding, N. C. Nogueira-de-Souza, P. H. Krebsbach, K. S. O'Shea, J. Lahann, G. D. Smith, *Nat. Biotechnol.* **2010**, *28*, 581.
- [11] L. T. H. Dang, N. T. Feric, C. Laschinger, W. Y. Chang, B. Zhang, G. A. Wood, W. L. Stanford, M. Radisic, *Biomaterials* **2014**, *35*, 7786.
- [12] J. R. Klim, L. Li, P. J. Wrighton, M. S. Piekarczyk, L. L. Kiessling, *Nat. Methods* **2010**, *7*, 989.
- [13] Z. Melkoumian, J. L. Weber, D. M. Weber, A. G. Fadeev, Y. Zhou, P. Dolley-Sonneville, J. Yang, L. Qiu, C. A. Priest, C. Shogbon, A. W. Martin, J. Nelson, P. West, J. P. Beltzer, S. Pal, R. Brandenberger, *Nat. Biotechnol.* **2010**, *28*, 606.
- [14] E. G. Z. Centeno, H. Cimarosti, A. Bithell, *Mol. Neurodegener.* **2018**, *13*, 27.
- [15] J. Lee, C. C. Rabbani, H. Gao, M. R. Steinhart, B. M. Woodruff, Z. E. Pfleum, A. Kim, S. Heller, Y. Liu, T. Z. Shipchandler, K. R. Koehler, *Nature* **2020**, *582*, 399.
- [16] G. Pettinato, S. Lehoux, R. Ramanathan, M. M. Salem, L. X. He, O. Muse, R. Flaumenhaft, M. T. Thompson, E. A. Rouse, R. D. Cummings, X. Wen, R. A. Fisher, *Sci. Rep.* **2019**, *9*, 8920.
- [17] M. M. Gepp, B. Fischer, A. Schulz, J. Dobringer, L. Gentile, J. A. Vásquez, J. C. Neubauer, H. Zimmermann, *J. Appl. Phycol.* **2017**, *29*, 2451.
- [18] S. M. Badenes, A. Fernandes-Platzgummer, C. A. V. Rodrigues, M. M. Diogo, C. L. Da Silva, J. M. S. Cabral, in *Stem Cell Manuf.* **2016**, 77.
- [19] V. C. Chen, S. M. Couture, J. Ye, Z. Lin, G. Hua, H.-I. P. Huang, J. Wu, D. Hsu, M. K. Carpenter, L. A. Couture, *Stem Cell Res.* **2012**, *8*, 388.
- [20] G. Gao, T. Yonezawa, K. Hubbell, G. Dai, X. Cui, *Biotechnol. J.* **2015**, *10*, 1568.
- [21] S. Hong, D. Sycks, H. F. Chan, S. Lin, G. P. Lopez, F. Guilak, K. W. Leong, X. Zhao, *Adv. Mater.* **2015**, *27*, 4035.
- [22] M. T. Poldervaart, B. Goversen, M. de Ruijter, A. Abbadessa, F. P. W. Melchels, F. C. Öner, W. J. A. Dhert, T. Vermonden, J. Alblas, *PLoS One* **2017**, *12*, e0177628.
- [23] R. Suntornnond, J. An, C. K. Chua, *Macromol. Mater. Eng.* **2017**, *302*, 1600266.
- [24] L. Shi, H. Carstensen, K. Hözl, M. Lunzer, H. Li, J. Hilborn, A. Ovsianikov, D. A. Ossipov, *Chem. Mater.* **2017**, *29*, 5816.
- [25] A. Skardal, M. Devarasetty, H. W. Kang, I. Mead, C. Bishop, T. Shupe, S. J. Lee, J. Jackson, J. Yoo, S. Soker, A. Atala, *Acta Biomater.* **2015**, *25*, 24.
- [26] M. Di Giuseppe, N. Law, B. Webb, R. A. Macrae, L. J. Liew, T. B. Sercombe, R. J. Dilley, B. J. Doyle, *J. Mech. Behav. Biomed. Mater.* **2018**, *79*, 150.
- [27] S. M. Hull, C. D. Lindsay, L. G. Brunel, D. J. Shiawski, J. W. Tashman, J. G. Roth, D. Myung, A. W. Feinberg, S. C. Heilshorn, *Adv. Funct. Mater.* **2020**, *31*, 2007983.
- [28] Y. Li, X. Jiang, L. Li, Z. N. Chen, G. Gao, R. Yao, W. Sun, *Biofabrication* **2018**, *10*, 044101.
- [29] F. Salaris, A. Rosa, *Brain Res.* **2019**, *1723*, 146393.
- [30] H. Huang, J. Shi, J. Laskin, Z. Liu, D. S. McVey, X. S. Sun, *Soft Matter* **2011**, *7*, 8905.
- [31] X. Shen, X. Mo, R. Moore, S. J. Frazier, T. Iwamoto, J. M. Tomich, X. S. Sun, *J. Nanosci. Nanotechnol.* **2006**, *6*, 837.
- [32] H. Huang, A. I. Herrera, Z. Luo, O. Prakash, X. S. Sun, *Biophys. J.* **2012**, *103*, 979.
- [33] X. S. Sun, H. Huang, *US Patent 8,835,395* **2014**.
- [34] S. Thippabhotla, C. Zhong, M. He, *Sci. Rep.* **2019**, *9*, 13012.
- [35] Y. Lei, D. V. Schaffer, *Proc. Natl. Acad. Sci. U. S. A.* **2013**, *110*, E5048.
- [36] K. G. Chen, B. S. Mallon, R. D. G. McKay, P. G. Robey, *Cell Stem Cell* **2014**, *14*, 13.
- [37] S. N. Brimble, E. S. Sherrer, E. W. Uhl, E. Wang, S. Kelly, A. H. Merrill, A. J. Robins, T. C. Schulz, *Stem Cells* **2007**, *25*, 54.
- [38] W. A. Pastor, D. Chen, W. Liu, R. Kim, A. Sahakyan, A. Lukianchikov, K. Plath, S. E. Jacobsen, A. T. Clark, *Cell Stem Cell* **2016**, *18*, 323.
- [39] A. Morshed, M. S. Noghabi, P. Dröge, *Stem Cell Rev.* **2013**, *9*, 523.
- [40] M. K. Ramlee, J. Wang, W. X. Toh, S. Li, *Genes (Basel)* **2016**, *7*, 50.
- [41] C.-C. Tsai, C.-L. Chen, H.-C. Liu, Y.-T. Lee, H.-W. Wang, L.-T. Hou, S.-C. Hung, *J. Biomed. Sci.* **2010**, *17*, 64.
- [42] M.-Y. Son, H. Choi, Y.-M. Han, Y. S. Cho, *Stem Cells* **2013**, *31*, 2374.
- [43] K. C. Lee, W. K. Wong, B. Feng, *Biomedicines* **2013**, *1*, 49.
- [44] S. Masui, S. Ohtsuka, R. Yagi, K. Takahashi, M. S. H. Ko, H. Niwa, *BMC Dev. Biol.* **2008**, *8*, 45.
- [45] K. B. Scotland, S. Chen, R. Sylvester, L. J. Gudas, *Dev. Dyn. Off. Publ. Am. Assoc. Anat.* **2009**, *238*, 1863.
- [46] A. Mohyeldin, T. Garzón-Muvdi, A. Quiñones-Hinojosa, *Cell Stem Cell* **2010**, *7*, 150.
- [47] P. Rebuzzini, M. Zuccotti, C. A. Redi, S. Garagna, *Cytogenet. Genome Res.* **2015**, *147*, 1.
- [48] M. Pawlak, R. Jaenisch, *Genes Dev.* **2011**, *25*, 1035.
- [49] Y. Nakashima, T. Omasa, *BioRes. Open Access* **2016**, *5*, 84.
- [50] A. Laperle, C. Hsiao, M. Lampe, J. Mortier, K. Saha, S. P. Palecek, K. S. Masters, *Stem Cell Rep.* **2015**, *5*, 195.
- [51] C. M. Madl, S. C. Heilshorn, H. M. Blau, *Nature* **2018**, *557*, 335.
- [52] C. M. Madl, B. L. Lesavage, R. E. Dewi, C. B. Dinh, R. S. Stowers, M. Khariton, K. J. Lampe, D. Nguyen, O. Chaudhuri, A. Enejder, S. C. Heilshorn, *Nat. Mater.* **2017**, *16*, 1233.

- [53] A. S. Fanning, J. M. Anderson, *J. Clin. Invest.* **1999**, *103*, 767.
- [54] B. A. Hemmings, D. F. Restuccia, *Cold Spring Harb. Perspect. Biol.* **2012**, *4*, a011189.
- [55] A. M. Hossini, A. S. Quast, M. Plötz, K. Grauel, T. Exner, J. Küchler, H. Stachelscheid, J. Eberle, A. Rabien, E. Makrantonaki, C. C. Zouboulis, *PLoS One* **2016**, *11*, e0154770.
- [56] T. Kimura, T. Nakano, in *Regul. Networks Stem Cells* (Eds: V. K. Rajasekhar, M. C. Vemuri), Humana Press **2009**, pp. 309–318.
- [57] L. Romorini, X. Garate, G. Neiman, C. Luzzani, V. A. Furmento, A. S. Guberman, G. E. Seylever, M. E. Scassa, S. G. Miriuwa, *Sci. Rep.* **2016**, *6*, 35660.
- [58] Y.-G. Chen, Z. Li, X.-F. Wang, *Cell Stem Cell* **2012**, *10*, 231.
- [59] L. Armstrong, O. Hughes, S. Yung, L. Hyslop, R. Stewart, I. Wappler, H. Peters, T. Walter, P. Stojkovic, J. Evans, M. Stojkovic, M. Lako, *Hum. Mol. Genet.* **2006**, *15*, 1894.
- [60] T.-S. Huang, L. Li, L. Moalim-Nour, D. Jia, J. Bai, Z. Yao, S. A. L. Bennett, D. Figeys, L. Wang, *Stem Cells* **2015**, *33*, 1419.
- [61] G. Ramazzotti, S. Ratti, R. Fiume, M. Y. Follo, A. M. Billi, I. Rusciano, E. O. Obeng, L. Manzoli, L. Cocco, I. Faenza, *Int. J. Mol. Sci.* **2019**, *20*, 2026.
- [62] Y. Xu, X. Zhu, H. S. Hahm, W. Wei, E. Hao, A. Hayek, S. Ding, *Proc. Natl. Acad. Sci. U. S. A.* **2010**, *107*, 8129.
- [63] Y. Hayashi, M. K. Furue, *Stem Cells Int.* **2016**, *2016*, 5380560.
- [64] F. Soncin, C. M. Ward, *Genes (Basel)* **2011**, *2*, 229.
- [65] G. De Santis, S. Miotti, M. Mazzi, S. Canevari, A. Tomassetti, *Oncogene* **2009**, *28*, 1206.
- [66] L. Li, S. A. L. Bennett, L. Wang, *Cell Adhes. Migr.* **2012**, *6*, 59.
- [67] Y. Shao, J. Sang, J. Fu, *Biomaterials* **2015**, *52*, 26.
- [68] C. McKee, C. Brown, G. R. Chaudhry, *Cells* **2019**, *8*, 1650.
- [69] G. Brusatin, T. Panciera, A. Gandin, A. Citron, S. Piccolo, *Nat. Mater.* **2018**, *17*, 1063.
- [70] I. M. Moya, G. Halder, *Nat. Rev. Mol. Cell Biol.* **2019**, *20*, 211.
- [71] S. Dupont, in *Hippo Pathw. Methods Protoc. Methods Mol. Biol.* (Ed: A. Hergovich), Humana Press Inc. **2019**, pp. 183–202.
- [72] S. Lee, A. E. Stanton, X. Tong, F. Yang, *Biomaterials* **2019**, *202*, 26.
- [73] F. Rey, B. Barzaghi, A. Nardini, M. Bordoni, G. V. Zuccotti, C. Cereda, M. T. Raimondi, S. Carelli, *Cells* **2020**, *9*, 1636.
- [74] G. Ying, N. Jiang, C. Yu, Y. S. Zhang, *Bio-Des. Manuf.* **2018**, *1*, 215.
- [75] J. Gong, C. C. L. Schuurmans, A. M. van Genderen, X. Cao, W. Li, F. Cheng, J. J. He, A. López, V. Huerta, J. Manríquez, R. Li, H. Li, C. Delavaux, S. Sebastian, P. E. Capendale, H. Wang, J. Xie, M. Yu, R. Masereeuw, T. Vermonden, Y. S. Zhang, *Nat. Commun.* **2020**, *11*, 1.
- [76] Q. Gu, E. Tomaskovic-Crook, G. G. Wallace, J. M. Crook, *Adv. Healthcare Mater.* **2017**, *6*, 1700175.
- [77] D. Nguyen, D. A. Hgg, A. Forsman, J. Ekholm, P. Nimkingratana, C. Brantsing, T. Kalogeropoulos, S. Zaunz, S. Concaro, M. Brittberg, A. Lindahl, P. Gatenholm, A. Enejder, S. Simonsson, *Sci. Rep.* **2017**, *7*, 658.
- [78] E. Abelseth, L. Abelseth, L. De La Vega, S. T. Beyer, S. J. Wadsworth, S. M. Willerth, *ACS Biomater. Sci. Eng.* **2019**, *5*, 234.
- [79] Y. Loo, A. Lakshmanan, M. Ni, L. L. Toh, S. Wang, C. A. E. Hauser, *Nano Lett.* **2015**, *15*, 6919.
- [80] A. Faulkner-Jones, C. Fyfe, D. J. Cornelissen, J. Gardner, J. King, A. Courtney, W. Shu, *Biofabrication* **2015**, *7*, 044102.
- [81] L. Koch, A. Deiwick, A. Franke, K. Schwanke, A. Haverich, R. Zweigerdt, B. Chichkov, *Biofabrication* **2018**, *10*, 035005.